

Influence of torsional waves in solar magnetic flux tubes on spectral lines

S.R.O. Ploner and S.K. Solanki

Institut für Astronomie, ETH-Zentrum, CH-8092 Zürich, Switzerland

Received 6 October 1998 / Accepted 25 February 1999

Abstract. The influence of torsional waves propagating along a thin, vertical, photospheric flux tube on Zeeman-split polarized line profiles (Stokes profiles) is investigated using a simple MHD model. In the presence of such a wave *spatially resolved* Stokes profiles are found to oscillate strongly in wavelength, amplitude and blue-red asymmetry. Qualitatively, torsional waves induce similar changes into the line profiles as kink waves (Ploner & Solanki 1997). The magnitude of the line parameter variation depends strongly on the observed location with respect to the flux-tube axis.

The *spatially averaged* Stokes V and Q profiles are found to follow the torsional wave with double the wave frequency, some parameters of Stokes U fluctuate directly at the wave frequency, however. The other main feature of the spatially averaged profiles is their comparatively small reaction to the wave. The reason for the latter is that most polarized light is produced near the centre of the flux tube where, however, the torsional wave produces only weak perturbations.

Temporally and spatially averaged Stokes profiles are found to be only negligibly shifted, but strongly broadened. The sign of the small remaining asymmetry is opposite in Stokes Q to that in V and U . The amplitude of the wave and the location of the flux tube on the solar disk have a strong influence on the magnitude of the perturbation of the Stokes profiles.

Key words: Magnetohydrodynamics (MHD) – radiative transfer – waves – Sun: faculae, plages – Sun: magnetic fields – Sun: photosphere

1. Introduction

The details of the chromospheric and coronal heating processes have been the subject of long and intense study. Among others, a variety of processes have been proposed in which MHD waves in small magnetic flux tubes channel the energy flux from below into the chromosphere and still higher layers (see the reviews by Narain & Ulmschneider 1990, 1996). One aspect of the investigation into these processes deals with the generation of flux-tube waves by turbulent motions in the outer convec-

tion zone. For example, Ulmschneider & Musielak (1998) investigated the generation of longitudinal tube waves, Huang et al. (1995) the generation of kink waves, while Anton (1989) studied the interaction between vortical flows and flux tubes, a process which gives rise to torsional waves. Another aspect has to do with the transport of kinetic energy through the photosphere by MHD-waves (e.g. Webb & Roberts 1980, Ziegler & Ulmschneider 1997a,b). The final aspect is the dissipation of the wave energy, e.g. by shock waves in the chromospheric layers in the case of longitudinal tube waves (e.g. Herbold et al. 1985, Fawzy et al. 1998) or through such mechanisms as mode coupling (e.g. Zähringer & Ulmschneider 1987), phase mixing (e.g. Nakariakov et al. 1997) and resonant absorption (e.g. Poedts et al. 1994) in the case of Alfvénic wave modes.

Observational evidence for the contribution of flux-tube waves to chromospheric or coronal heating is difficult to obtain and correspondingly poor (however, see Venkatakrishnan 1993). One possibility is to try to observe the propagating waves in the photosphere by means of polarization measurements. The problem with this approach is that little is known about the expected signature of such waves, in particular of the torsional Alfvén waves. The aim of the current paper is to provide some of the missing information. We use a simple model of torsional waves propagating along flux tubes to predict their signature in the polarized radiation of Zeeman-split lines.

Our model relies on the assumption that the flux tubes are small in diameter. This is thought to be satisfied for most flux tubes forming the solar magnetic network and active region plages. Consequently, the large variety of flux-tube modes (Roberts & Ulmschneider 1996) reduces to three (Spruit 1982), a compressible longitudinal (“sausage” mode) and two incompressible transverse modes (kink and torsional waves). The polarization signature of sausage modes has been investigated at solar disc centre by Solanki & Roberts (1992), that of kink waves by Ploner & Solanki (1997) at various positions on the disc. This paper is consequently dedicated to torsional waves. Other investigations that use theory in order to predict the influence of wave-like dynamic phenomena in flux tubes on spectral lines have been carried out by, e.g., Rammacher & Ulmschneider (1989), Rammacher (1991) and Steiner et al. (1995, 1996), but none of them considers torsional waves. In addition, techniques of polarimetric measurements are rapidly improving (e.g. Povel

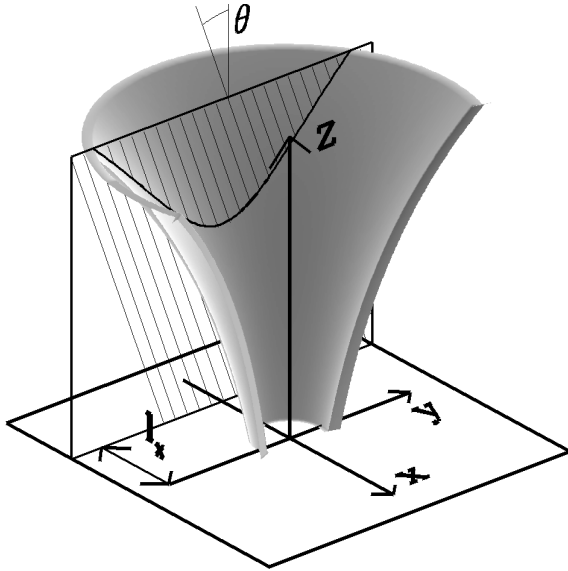


Fig. 1. Illustration of the model flux tube and a plane containing rays parallel to the line-of-sight. The shaded surface represents the boundary between the outer, field-free and inner, magnetized plasma. As an illustration a plane intersecting the flux tube at the location $x = l_x$ is shown. The plane contains mutually parallel rays pointing towards the observer located at heliocentric angle θ .

1995, Gandorfer & Povel 1997), in particular for the observation of dynamic phenomena (Solanki 1996, Ulrich 1996, Martínez Pillet et al. 1997, cf. Frutiger & Solanki 1998) giving a certain timeliness to investigations like the present one.

2. The model

This section introduces the model which underlies the present calculations. Basically, the method agrees with that used for the investigation of kink waves by Ploner & Solanki (1997, henceforth called Paper I) and details can be found there. Here we concentrate on aspects unique to torsional waves. We begin with an overview of the 3-D geometrical situation (Sect. 2.1), proceed with the description of torsional waves (Sect. 2.2) and end with basic symmetry considerations of torsional waves in a flux tube (Sect. 2.3), which turn out to be important for the interpretation of the synthesized line profiles.

2.1. Overview

Fig. 1 provides an overview of the model flux tube and fixes Cartesian coordinates (x, y, z) , of which z describes the height in the atmosphere. A part of the axially symmetric flux-tube boundary which separates the inner magnetized from the outer field-free atmosphere is represented by the shaded surface around z . In a first step, the *static* equilibrium flux tube is determined by horizontal pressure balance (using the zeroth-order thin flux-tube approximation, e.g. Ferriz Mas et al. 1989)

$$p_{ex} = p + \frac{B_z^2}{8\pi}, \quad (1)$$

where p_{ex} and p are respectively the outer and inner zeroth-order, i.e. unperturbed, gas pressure, and B_z is the zeroth-order vertical magnetic field. Both the pressure and the magnetic field decrease with increasing height and magnetic flux conservation causes the flux tube to expand with height.

For both the internal and external atmosphere we employ empirical models in order to obtain realistic polarized line profiles. The internal atmosphere used here is the plage flux-tube model of Solanki & Brigljević (1992), while the external atmosphere is the empirical quiet-sun model of Maltby et al. (1986). Note, however, that the perturbation is calculated for an isothermal atmosphere (see Sect. 2.2). Following Rüedi et al. (1992) the magnetic field strength is chosen to be 1500 G at $z = 0$ ($z = 0$ marks the layer at which optical depth $\tau = 1$ at $\lambda = 5000 \text{ \AA}$ in the quiet sun). The flux-tube radius at $z = -261 \text{ km}$ (the lower boundary of the calculation domain) is $R_0 \sim 85 \text{ km}$, resulting in a radius of 100 km at $z = 0$. The upper boundary of the domain lies at $z = 700 \text{ km}$.

In a second step, the perturbations to the magnetic and velocity vectors due to the torsional wave are added to the zeroth-order quantities of the inner atmosphere (see Sect. 2.2). The flux tube is then intersected by y - z planes equally spaced in the x -direction. In Fig. 1 a plane located at $x = l_x$ is shown, where l_x is the distance to the flux-tube axis along the x -direction. Each plane contains a number of mutually parallel rays (lines-of-sight) pointing towards the observer. Each ray is inclined by the heliocentric angle θ to the vertical. The atmosphere along each ray is determined on a grid with constant τ -spacing (see Bunte et al. 1993).

Finally, the equations of polarized radiative transfer are numerically integrated along each ray using the Stokes formalism. This calculation provides us with the line profiles in Stokes I (total intensity), Stokes V (net circular polarization) as well as Stokes Q and U (net linear polarizations). In a first part of the subsequent analysis we investigate the Stokes profiles which stem from a fixed plane, i.e. for a given $l_x = \text{const}$. Then signals resulting from spatially and later also temporally averaged line profiles are considered.

For details of the calculation of atmospheric quantities along the rays or the subsequent integration of the radiative transfer equation we refer the interested reader to Bunte et al. (1993) and Paper I. The major change relative to Paper I consists of the inclusion of the 3-D flux-tube structure, which is dictated by the nature of torsional waves whose line-of-sight velocity component is largest at large x (Sect. 2.3).

2.2. Torsional waves

Torsional waves in axially symmetric flux tubes are best described in cylindrical coordinates r (radial distance from flux-tube axis), φ (azimuthal angle) and z (height, see Fig. 1.). We consider linear, azimuthally symmetric (i.e. with no explicit φ -dependence) waves in the thin flux-tube approximation (e.g. Ferriz Mas et al. 1989). Zhugzhda (1996) found a way to close the linearized system of equations including radial expansion terms up to second order (Ferriz Mas et al. 1989). Those equa-

tions are particularly simple for a non-rotating and untwisted flux tube. In this case the azimuthal components of the momentum and induction equations separate out from the remaining magneto-hydrodynamic equations and read

$$4\pi\rho\partial_t(v_{\varphi 1}) = B_{\varphi 1}\partial_z(B_z) - B_z\partial_z(B_{\varphi 1}), \quad (2)$$

$$\partial_t(B_{\varphi 1}) = B_z\partial_z(v_{\varphi 1}), \quad (3)$$

respectively. Here, ρ and B_z are the zeroth order components of the density and vertical magnetic field, respectively, and $v_{\varphi 1}$ and $B_{\varphi 1}$ are first order disturbances to the azimuthal components of the velocity and magnetic field, respectively. Finally, ∂_a stands for $\partial/\partial a$ with a being an arbitrary coordinate. For an isothermal atmosphere (i.e. $\rho \sim \exp(-z/H)$ and $B_z \sim \exp(-z/2H)$, with H the pressure scale height) Eqs. (2) and (3) possess the following solution:

$$v_{\varphi} = rv_{\varphi 1} = r\tilde{v}\exp(i(\omega t - k_z z)), \quad (4)$$

$$B_{\varphi} = rB_{\varphi 1} = r\tilde{B}_{\varphi}\exp\left(i(\omega t - k_z z) - \frac{z}{2H}\right), \quad (5)$$

$$\tilde{v}/v_A = -B_{\varphi 1}/B_z, \quad (6)$$

$$\omega = k_z v_A, \quad (7)$$

where t is the time (or phase) and $v_A = B_z/\sqrt{4\pi\rho}$ the (constant) Alfvén speed. Eq. (7) is the dispersion relation between the frequency ω and wavenumber k_z of a pure Alfvén wave. The torsional wave described by Eqs. (4) and (5) is determined by specifying the wave frequency ω and angular velocity \tilde{v} (which determines the constant \tilde{B}_{φ} through $B_{\varphi 1}$ in Eq. 6). Note that the phase shift (Eq. 6) between velocity and azimuthal field is constant and agrees with the expectations for upward propagating Alfvén waves. It also agrees with the case of high frequency kink waves (Paper I), which is responsible for some of the similarities in observational signature.

As in Paper I we disturb the equilibrium flux tube, whose stratification is described by a realistic model atmosphere, with an isothermal torsional wave. The employed Alfvén speed is $v_A = 12.6 \text{ km s}^{-1}$ and the scale height is $H = 128 \text{ km}$. These parameter values correspond to those of the equilibrium flux tube at the lower boundary of the estimated height range of line formation ($z \sim 50 \text{ km}$). We again justify this approximation by noting that the deviation from an isothermal atmosphere within the height range of line formation generally is rather small. Strictly speaking, the use of isothermal torsional waves limits the wavelength to be smaller than the temperature scale height. For oscillations with larger wavelengths the temperature stratification, e.g. in the upper atmosphere, becomes important. Partial reflection caused by a temperature increase or effects due to merging flux tubes may influence the wave properties in the height range of line formation. But note, that we are only interested in the principal changes of the atmosphere due to torsional waves and neglect to model comprehensively the wave propagation. We therefore do not take the restriction to short wavelength too serious and go beyond this limit. Larger wavelengths are of interest because they provide a constant phase with height and allow us to separate the effects introduced by the wave frequency.

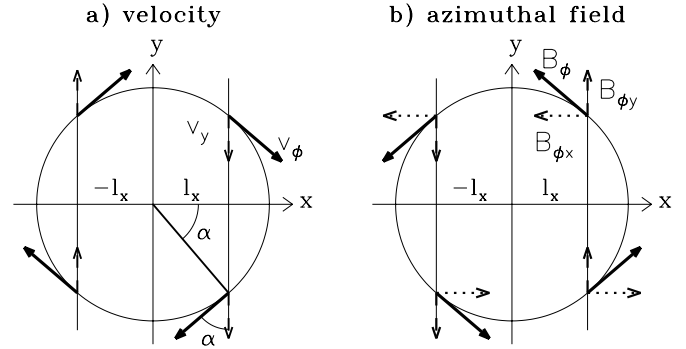


Fig. 2a and b. Illustration of how azimuthal disturbances of a torsional wave are projected onto a horizontal plane. The circles represent horizontal cuts through the flux tube seen in Fig. 1 and the vertical lines parallel to y symbolize two intersections of these cuts with planes at locations $\pm l_x$. This figure illustrates that the component of the horizontal velocity, v_y frame **a** and the projection in the y -direction of the azimuthal component of the magnetic field, $B_{\varphi y}$ frame **b** are proportional to l_x and do not depend upon y .

Additional limitations are introduced by the thin flux-tube approximation. The radial expansion of the equations underlying this approximation forces us to consider wavelengths that are large compared to the flux-tube radius. Note that this radius increases exponentially with height, so that this requirement is increasingly poorly fulfilled in the upper atmosphere. However, as mentioned above the less realistically modeled upper part of the flux tube does not significantly influence the spectral lines, which obtain their main contribution at smaller height.

2.3. Symmetry properties

In Sect. 3 we first investigate the effect of torsional waves on polarized profiles generated in a single plane (see Fig. 1). Torsional waves cause r -dependent changes within the flux tube which give rise to y - and x -dependences from the vantage points of an observer located in the y - z plane. It is therefore necessary to discuss the changes induced by the wave and the symmetries the changes may possess along individual rays. Because the flux tube harbouring the torsional wave is assumed to be vertical, the wave-induced changes, v_{φ} and B_{φ} , lie in a horizontal plane. So in a first step, in order to simplify explanations, we consider only a single horizontal plane and work out in it the horizontal velocity and magnetic components parallel and perpendicular to a hypothetical horizontal line-of-sight. Only after that do we take into account that the rays are inclined to the horizontal.

The circles in Fig. 2 represent horizontal cuts through the flux tube (compare with Fig. 1). For illustrative purposes they are intersected by two planes symbolized by the two vertical lines located at $\pm l_x$. Of the wave's velocity v_{φ} only its component in the y -direction, v_y , is relevant (because only $v_y \sin \theta$, the line-of-sight velocity, enters the transfer equation). Fig. 2a shows that v_y changes sign between the planes at $\pm l_x$ (at a fixed time t):

$$v_y(t, l_x) = -v_y(t, -l_x). \quad (8)$$

In other words, an observer sees a line-of-sight velocity in one half of the flux tube ($l_x < 0$) that is directed oppositely to that in the other half ($l_x > 0$). This result is independent of θ (except $\theta = 0$). Half a wave period later v_φ reverses its direction again giving rise to a change in sign of v_y ,

$$v_y(t, l_x) = -v_y\left(t + \frac{T}{2}, l_x\right), \quad (9)$$

where $T = 2\pi/\omega$ is the wave period. In addition, v_y is independent of y for a fixed l_x , as follows from

$$v_y = v_\varphi \cos \alpha = v_\varphi r \cos \alpha = v_\varphi l_x, \quad (10)$$

i.e. along a horizontal ray the line-of-sight velocity remains constant within the flux tube. In Eq. (10) we have made use of the fact that α is the angle between v_φ and v_y as well as between r and l_x . The magnitude of v_y is consequently proportional to l_x and the line profiles formed in the outermost parts of the flux tube are expected to exhibit the largest reaction to the wave.

The situation for the magnetic field is far more complex than for the velocity, since in addition to the wave-induced B_φ component time independent B_z and B_r components are also present, all of which affect the polarization state. Consider first the azimuthal component, B_φ , of the magnetic field generated by the torsional wave (Fig. 2b). Note that according to Eq. (6) $B_{\varphi y}$ is directed oppositely to v_y . Eqs. (8) to (10) found for v_y are also valid for $B_{\varphi y}$. $B_{\varphi x}$ (which influences Stokes Q and U) has the same sign on $l_x < 0$ and $l_x > 0$ whereas it changes sign along y . The dominant component in the photosphere is B_z . It is almost an order of magnitude larger than the other components. In order to estimate the relative significance of B_r and B_φ we first note that at the height of line formation ($z \sim 50$ km) and at the flux-tube boundary the expansion of the magnetic field with height results in $B_r/B_z \sim 0.2$. The field inclination due to the wave B_φ/B_z is a factor of 2 smaller there (assuming a velocity amplitude of $\tilde{v}R_0 \sim 1$ km s $^{-1}$) because of the comparatively high Alfvén speed (Eq. 6). Hence the wave superimposes relatively small changes B_φ onto the static field (B_z and B_r). Note that the radial field B_r has the opposite symmetry properties relative to x and y (B_{rx} behaves like $B_{\varphi y}$ and B_{ry} like $B_{\varphi x}$) and it modifies the symmetry noted above because $B_{rx} > B_{\varphi x}$.

In the Stokes formalism the orientation of the magnetic field enters the radiative transfer through the angles γ (the inclination between field vector and line-of-sight) and χ (azimuth, measured in a plane perpendicular to the line-of-sight). Examples of $\gamma(y)$ and $\chi(y)$ are displayed in Fig. 3 for a flux tube with (dotted lines) and without (solid lines) a twist such as that introduced by a torsional wave ($B_\varphi/B_z = 0.1$). In order to illustrate the main effects clearly, all quantities have been assumed to be height independent when making these figures (but not in the rest of the paper). In the plotted case the flux tube is seen at $\theta = 70^\circ$. Fig. 3a shows that in the static case γ is smaller than θ for $y < 0$ (i.e. for locations of the flux tube nearer the observer), whereas $\gamma > \theta$ for $y > 0$ (located in the flux tube away from the observer). This reflects the combined effects of B_z and B_{ry} . Note that γ is the same on both halves of the flux tube (thick

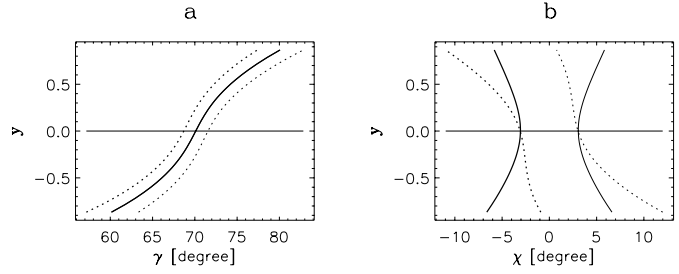


Fig. 3a and b. Dependence of γ and χ on y and l_x , where γ is the angle between the magnetic field vector and the line-of-sight, and χ is the magnetic azimuth relative to the line-of-sight. Displayed is the situation along 2 horizontal cuts through a flux tube observed at an angle of $\theta = 70^\circ$ to the vertical. The thick and thin lines correspond to $-l_x$ and l_x , respectively. The solid curves display the time-independent magnetic field with components B_z and B_r (the thick and thin curves are identical in frame a) The dotted curves result when the twist due to a torsional wave, B_φ , is included. Frame a shows that the broad range of γ along y is caused by B_r whereas the wave only affects γ weakly (indicated by the difference between the thick and thin dotted lines). It follows from frame b that the sign of χ is coupled to the sign of l_x .

and thin curves corresponds to $l_x > 0$ and $l_x < 0$ in Fig. 3). The sign of χ , however, corresponds to the sign of l_x which is due to B_{rx} . The changes caused by the wave can be judged from the difference between the solid and dotted lines.

3. Results

In this section we investigate the signature of torsional waves in polarized line profiles. We consider both time resolved and time averaged line profiles. To begin with (in Sect. 3.1) we discuss basic features of the line profiles generated in single, vertical planes cutting through the flux tube, such as the plane shown in Fig. 1. Because of the difference in behaviour we discuss Stokes V and Q (Sect. 3.2) separately from Stokes U (Sect. 3.3). The Stokes I profile is not discussed since the torsional wave mode only has a minute influence on it.

In Sects. 3.1 to 3.3 we consider the effect on the spectral line Fe I 5250 Å at the heliocentric angle $\theta = 60^\circ$ of a single type of wave having $\omega = 0.04$ Hz (which corresponds to a period of $T \sim 2.6$ Min and a wavelength of approximately 2000 km) and amplitude $\tilde{v} = 1$ km at R_0 . Such a low frequency and long wavelength was chosen in order to ensure that the wave phase remains constant over the range of formation of Fe I 5250 Å. This spectral line has a Landé-factor $g = 3$ and was already employed in the study of kink waves in Paper I. Finally, the dependence of the signature of torsional waves on the characteristics of the wave (ω and \tilde{v}), the location on the solar disc (θ) and the chosen spectral line is discussed in Sect. 3.4. In that section we also consider the Fe I 5083 Å line, which is stronger than Fe I 5250 Å and which showed a larger influence of kink waves in Paper I.

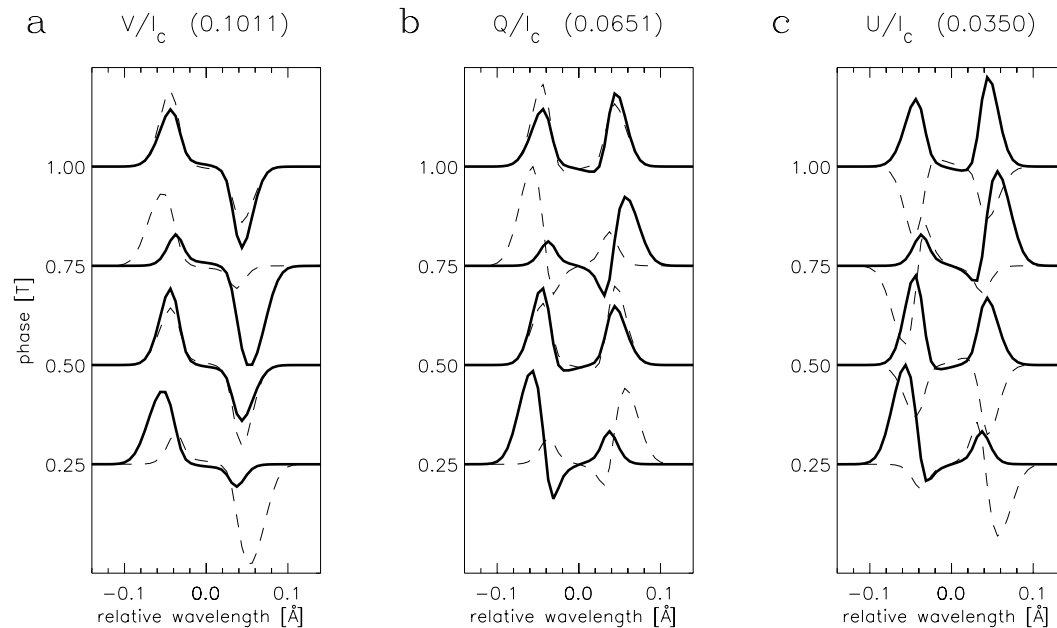


Fig. 4a–c. Stack-plot of Stokes V **a**, Stokes Q **b** and Stokes U **c** profiles of Fe I 5250.2 Å displayed at 4 phases spanning a wave period ($\omega = 0.04\text{Hz}$, $T \approx 2.6\text{ min}$, $\lambda \approx 2000\text{ km}$ and $\tilde{v} = 1\text{ km s}^{-1}$). The thick solid lines represent the Stokes profiles formed along rays lying in the plane at $l_x = 100\text{ km}$ whereas the thin dashed lines refer to $l_x = -100\text{ km}$. The numbers in brackets at the top of each frame are the maximum amplitudes reached by the signal in that frame. They corresponds to the amount by which the profiles at one phase are offset to the next in the figure. Phase 0.25 corresponds to the situations plotted in Figs. 2 and 3.

3.1. Polarized line profiles

Fig. 4 shows a stack plot of Stokes V , Q and U generated in a flux tube supporting a torsional wave. The displayed profiles are formed in two planes lying at a distance of $l_x = \pm 100\text{ km}$ from the flux-tube axis (solid and dashed profiles in Fig. 4, respectively). From bottom to top the profiles correspond to 4 equally spaced phases or times covering a wave period T . We use the stellar convention in which phase runs from 0 to 1. Focus now on Stokes V generated in the plane at $l_x = +100$ (solid profiles in Fig. 4a). At phase 0.25 the profiles are seen to be blue-shifted and to have a larger blue than red lobe (leading to positive asymmetry, as defined in Appendix A). At phase 0.5 the profiles are more symmetric and almost unshifted. At phase 0.75 the profile has an asymmetry and shift opposite to phase 0.25 but with a larger total amplitude (see the end of Sect. 3.2.1). Finally, the situation at phase 1.0 is basically the same as that at 0.5 in the sense that both are near the unperturbed state. This description of the Stokes V evolution is also valid for Stokes Q (solid lines in Fig. 4 b) with the exception that the Stokes Q amplitude is small when Stokes V is large and vice versa, i.e. Stokes Q is somewhat stronger at phase 0.25 than at phase 0.75. In summary, the change in asymmetry, line shift and broadening is in phase between Stokes V and Q whereas that of the total amplitude is in antiphase. (Stokes U is discussed later in Sect. 3.3). Note also that the line profiles exhibit an oscillatory behaviour with the same period as the wave.

The time evolution of Stokes V and Q resembles the sequence generated by a kink wave, although the influence of the latter is larger (compare with Fig. 4 of Paper I). The similarity

between the profiles generated by torsional and kink waves is not astonishing: along a single plane the line-of-sight components of the velocity and magnetic field perturbations due to the torsional wave are similar to the distortions produced by a kink wave. This can be seen approximately from Fig. 2. A kink wave (which shakes the flux tube in the y -direction) generates B_y and v_y which are constant in x and y . The corresponding distortions $B_{\varphi y}$ and v_y due to a torsional wave are also constant along y , although not along x . The magnitude of both v_y and $B_{\varphi y}$ is proportional to l_x and therefore depends strongly on the location of the plane. Consequently, the influence of torsional waves on Stokes V and Q increases with increasing l_x . This dependence is to be discussed in the next section.

One other important difference between kink and torsional waves is that whereas kink waves cause the whole flux tube to oscillate in phase, torsional waves cause the left and right halves of the flux tube as seen from the observer (i.e. the parts $l_x > 0$ and $l_x < 0$ of the flux tube, see Fig. 1) to oscillate in antiphase (see Eq. 8). The result of this is seen in Fig. 4 by comparing the dashed profiles (corresponding to $l_x < 0$) with the solid ones ($l_x > 0$). The dashed Stokes V and Q profiles at phase 0.25 are nearly identical to their solid counterparts at phase 0.75 (see Eq. 9). The profiles differ slightly due to the magneto-optical effects (see Sect. 3.2.2).

3.2. Time evolution of Stokes V and Q

In this section we discuss the evolution of Stokes V and Q on the basis of selected line-profile parameters. The choice of the

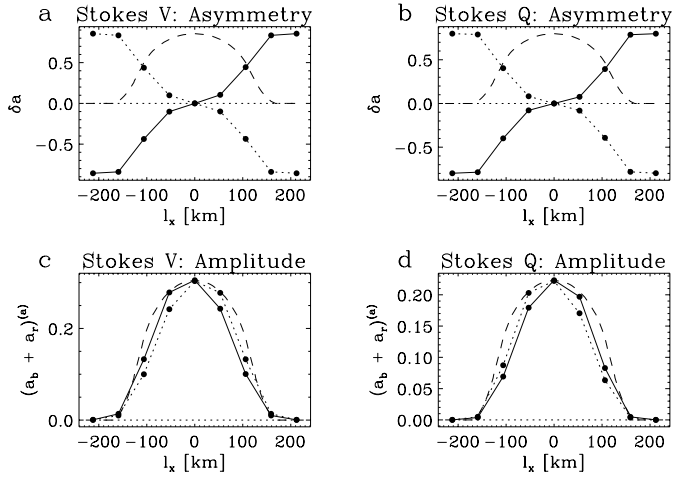


Fig. 5a–d. Amplitude a_σ and amplitude asymmetry δa of Stokes V **a** and **c** and Q **b** and **d** vs. l_x . The solid curve refers to phase $t = 0.25$ and the dotted to $t = 0.75$. The dashed curve displays the fractional area coverage of the magnetized plasma and is the same in all 4 frames (see text for details). The bullets mark the locations l_x of the planes containing the lines-of-sight. The underlying wave is the same as in Fig. 4. Note the increase of δa with increasing $|l_x|$, coupled with a rapid decrease of the amplitude. Also note that in the presence of the wave the amplitudes a_σ at $l_x > 0$ are not the same as for $l_x < 0$.

line-profile parameters is the same as in Paper I. The definitions of $\Delta\lambda_\sigma$ (line shift), $\Delta\lambda_{cg}$ (line broadening), a_σ (sum of the σ -component amplitudes) and δa and δA (relative amplitude and area asymmetry, respectively) are given in Appendix A.

3.2.1. Spatially resolved line profile parameters

Fig. 5 displays a_σ and δa of Stokes V and Q formed within a single plane versus the location of that plane, l_x , at the phases 0.25 and 0.75. Both Stokes parameters show no asymmetry at the central plane $l_x = 0$. But with increasing distance $|l_x|$ from the central plane the asymmetry reaches nearly 100% and reflects strongly distorted profiles. It is the presence of cospatial gradients of the magnetic field and line-of-sight velocity at the flux-tube boundary which is responsible for the production of the Stokes asymmetry (e.g. Grossmann-Doerth et al. 1989, see Paper I). Gradients of these quantities along the rays inside the flux tube are far smaller (certainly for the chosen wave frequency and heliocentric angle). The large asymmetry generated in planes with high l_x is due primarily to the increasing line-of-sight velocity component with l_x . This quantity vanishes in the plane $l_x = 0$ where no asymmetry is generated.

The opposite dependence on l_x is found for a_σ which decreases with increasing $|l_x|$. This reflects the fact that the larger the $|l_x|$ the smaller the area of intersection of the flux tube with the vertical plane containing the lines-of-sight. In order to estimate the fraction of magnetized plasma we determined the intersection area of the flux tube with the vertical plane within the height range of line formation (between $z = 50$ km and $z = 250$ km). The ratio of this area to the corresponding total

area in the computational domain is plotted versus l_x in Fig. 5 (dashed line) and agrees well with the decrease of a_σ .

Two relations are important to note. Firstly, at a given phase the V (and also Q) amplitudes at $l_x > 0$ differ from those at $l_x < 0$. This effect can already be seen in Fig. 4 by comparing the solid and dashed profiles, in particular at phases 0.25 and 0.75. Secondly, at a phase at which Stokes V is stronger for $l_x > 0$ than for $l_x < 0$, the opposite is the case for Stokes Q : it is weaker for $l_x > 0$ than for $l_x < 0$. The above described behaviour is due to the fact that a positive $B_{\varphi y}$ increases γ and consequently Stokes Q whereas a negative $B_{\varphi y}$ similarly enlarges the V amplitude. We shall return to this point when discussing spatially averaged profiles. Note that line shift, and to some extent also line width, exhibits a similar dependence on l_x as the asymmetry (not plotted).

3.2.2. Spatially averaged line profile parameters

Small flux tubes are generally not resolved by current telescopes. The wave signature in spatially averaged profiles is therefore also of interest. Consequently, we determine the parameters (Appendix A) of the spatially averaged Stokes profiles and study their time evolution over a wave period. Spatially averaged profiles are formed by averaging together the profiles from all planes (each of which is located at a different l_x). In general we have employed 9 planes. Tests based on the use of more planes indicate that this number is adequate.

The time evolution of the line profile parameters as seen at three positions on the disc ($\theta = 30^\circ, 60^\circ$ and 80° , represented by solid, dotted and dashed profiles, respectively) is plotted in Fig. 6. It shows, among other things, that all parameters evolve basically with double the wave frequency in both Stokes V and Q . This behaviour differs from the spatially resolved case (Fig. 4) and must therefore be a consequence of the spatial averaging. The following two points are of importance when considering this averaging.

Firstly, as evident from Fig. 5 only planes with $|l_x| \leq 100$ km give a significant contribution to the spatially averaged profiles (for the particular model flux tube chosen). This is the reason why, e.g., δa and δA of the spatially averaged profiles are not as large as for the kink wave studied in Paper I.

Secondly, as is evident from Figs. 4 and 5, profiles from opposite halves of the flux tube ($l_x < 0$ and $l_x > 0$) display opposite shifts and asymmetries at a given phase. When adding the profiles from the two halves together the shift and asymmetries are further reduced. They do not disappear due to the difference in V and Q amplitudes between the two halves (see Fig. 4 and the discussion at the end of Sect. 3.2.1). These differences in amplitude are largest at the phases 0.25 and 0.75. At those phases the line shift and asymmetry in each half also have the largest magnitude (due to the correlation between v_φ and B_φ inherent to Alfvén waves, see Eq. 6). Both these facts conspire to produce a peak at phases 0.25 and 0.75 in shifts and asymmetries of V and Q .

That these two peaks have the same sign (i.e. that both are generally maxima or minima) within a wave period reflects

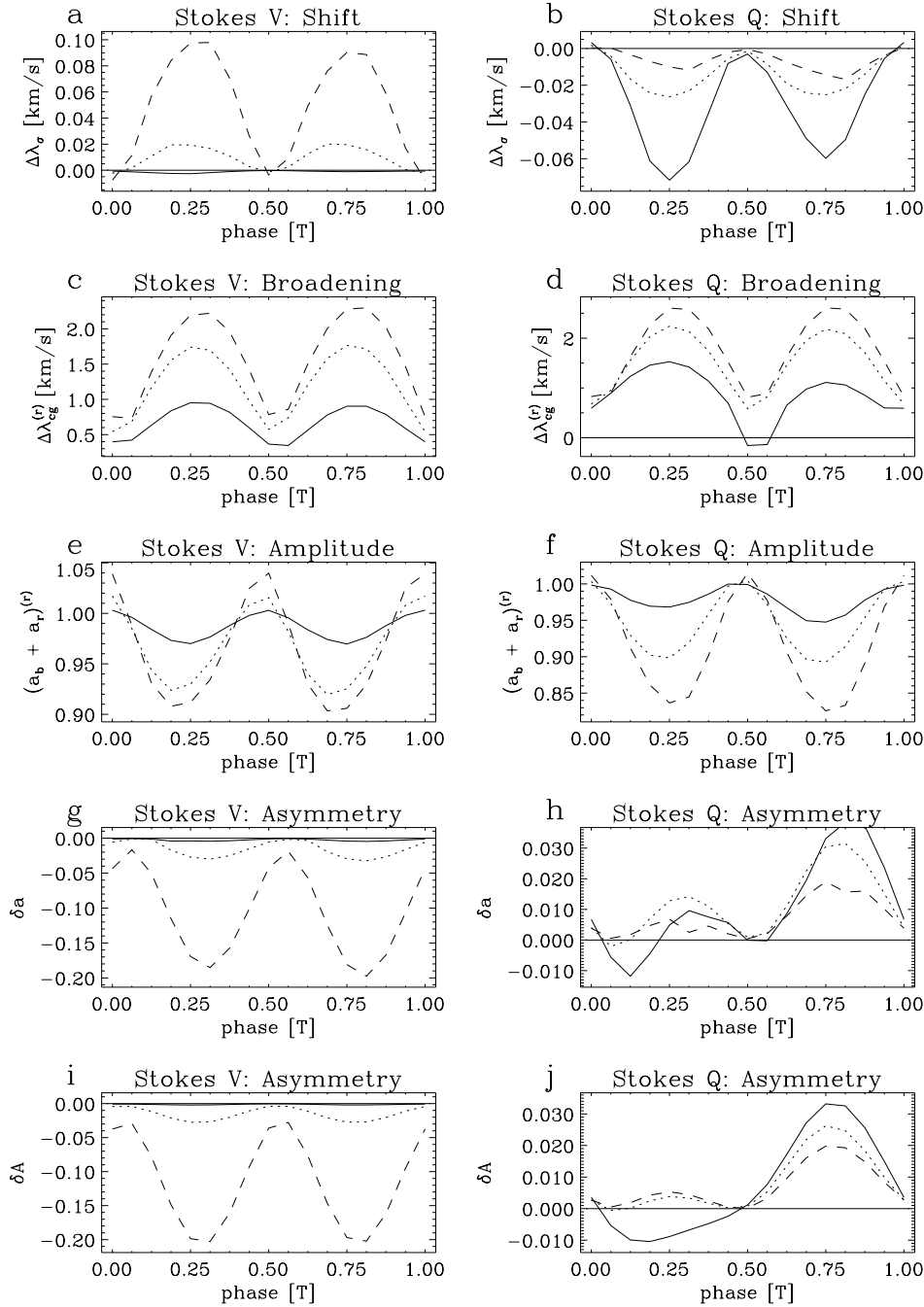


Fig. 6a–j. Parameters of spatially averaged Stokes V and Q profiles vs. phase. The plotted line profile parameters, indicated above each frame, are defined in Appendix A. The underlying wave is the same as in Fig. 5, but is now “observed” at three different disc positions corresponding to $\theta = 30^\circ$ (solid), $\theta = 60^\circ$ (dotted) and $\theta = 80^\circ$ (dashed). Note that all parameters oscillate with double the wave frequency.

the azimuthal symmetry of the wave. Note that to first order $V \sim \cos \gamma$ and $Q \sim (\sin \gamma)^2 \cos 2\chi$ and consequently both amplitudes do not depend on the sign of χ . After half a wave period the left and right halves of the flux tube are basically interchanged. For the magnetic field and velocity contributions of the torsional wave this fact has been shown with Eqs. 8 and 9 (where for instance $B_{\varphi x}$ has been neglected). The radial x -component of the background field, B_{rx} , changes sign from one half of the flux tube to the other. This leads to a corresponding change of sign in χ which to first order, however, does not affect Stokes V and Q . Then, after spatial averaging (and neglecting magneto-optical effects, see below) the phases t and $t + T/2$

are identical so that the resulting shift and asymmetry have the same sign at the peak values. Note the different origin of the doubled frequency in the line broadening. It is only affected by velocity magnitude whereas the sign of the velocity plays no role.

The evolution of the parameters differs between Stokes V and Q . The parameters $\Delta\lambda_\sigma$, δa and δA of Stokes V have the opposite sign to those of Q . Note first that at a given phase in one half of the flux tube the field is inclined towards the observer (i.e. small γ and large Stokes V), while in the other half it is inclined away (i.e. larger γ and large Stokes Q). Consequently, at a given phase the dominant V and Q signals emanate from

opposite halves of the flux tube (see Fig. 4). For a torsional wave the distortion of the magnetic field is in antiphase with that of the velocity which gives rise to opposite shifts at each phase in the different sides of the flux tubes. Because the dominating profiles of V and Q stem from opposite halves the antiphase between the field and velocity distortion gives rise to the opposite sign of the resulting shift of the spatially averaged profiles.

The area asymmetry δA is sensitive to the gradients along the line of sight of the magnetic field and velocity. The sign of the asymmetry is given by (Solanki & Pahlke 1988)

$$\text{sign}(\delta A) = \text{sign} \left(-\frac{\partial |B_{\text{los}}|}{\partial \tau} \frac{\partial v_{\text{los}}}{\partial \tau} \right) \quad (11)$$

Large gradients occur at locations where the line-of-sight enters or leaves the magnetized plasma. Using Fig. 2 it is seen that the gradients at both piercing points along a line-of-sight induce the same sign of δA but opposite signs in opposite halves of the flux tube, in accordance with Fig. 6.

Eye catching is the difference between the magnitudes at the two extremes of the Stokes Q parameters at phase 0.25 and 0.75, which is particularly pronounced in δa and δA (Figs. 6h and j). Stokes V parameters, in contrast, exhibit two almost equally strong peaks. As mentioned above, in the absence of magneto-optical effects the extrema at phases 0.25 and 0.75 are expected to be identical. This difference between the phases indeed vanishes if the radiative transfer is carried out without magneto-optical effects, as test calculations confirm. However, the largest Q profiles at phases 0.25 and 0.75 are generated in opposite halves of the flux tubes, i.e. at locations with opposite χ (see Fig. 4). Although the absorption coefficient of Stokes Q is not affected by this, the magneto-optical effects give a term that is sensitive to the sign of χ ($\varrho_Q \sim \sin 2\chi$), so that the two phases of the wave affect Stokes Q differently. For Stokes V , however, both phases remain identical (except for possible small effects that may appear due to the coupling between the various Stokes parameters in a realistic numerical solution, such as ours, of the Unno-Rachkovsky equations). For a more detailed discussion in the Milne-Eddington approximation see Appendix B.

According to Figs. 6e and f the normalized a_σ is below unity on the average, indicating that the profile amplitudes are decreased by the wave. Different processes play a role in determining $a_{\sigma,V}$ and $a_{\sigma,Q}$. The change of the inclination of the magnetic field vector due to the wave is one of them. However, a large part of the decrease in V and Q amplitudes is simply a compensation for the increased line width (Figs. 6c and d). The σ -component area $A_b + A_r$ (not shown) also oscillates, but with a considerably smaller relative amplitude, in support of this interpretation.

The line shift and the asymmetries of Stokes V show the opposite dependence on θ than the corresponding parameters of Stokes Q . Note that without net fluctuations in a_σ there would be no net fluctuations in the line shift and asymmetry (after averaging over the left and right halves of the flux tube) because all phases contribute equally to the spatial average. The larger the net fluctuations in a_σ the larger the difference of the contribution of various phases. The dependence on γ of the fluctuations

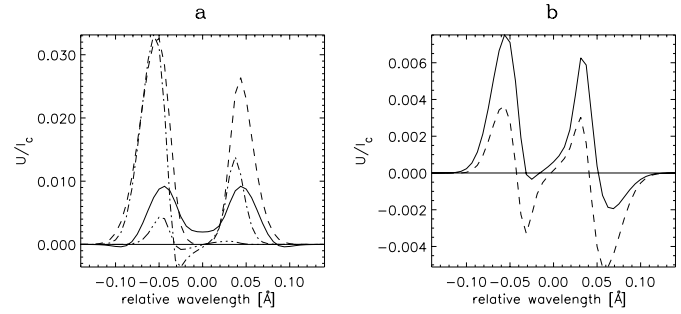


Fig. 7. **a** Stokes U profiles arising from planes located at $l_x = 0, 50, 100$ and 150 km (solid, dashed, dash-dotted and dash-triple dotted lines, respectively). The plotted profiles corresponds to phase 0.25 of the same wave as underlies Fig. 4. **b** The Stokes U profile spatially averaged over the whole flux tube. Solid curve: including magneto-optical effects, dashed curve: with magneto-optical effects switched off.

of a_σ is related to the relative sensitivity of Stokes Q and V : $\delta V/V \sim \tan \gamma$ and $\delta Q/Q \sim \cot \gamma$ (cf. Paper I). Consequently, changes in a_σ within a wave period are large for V near the solar limb but near disc centre for Stokes Q .

3.3. Time evolution of Stokes U

The evolution of Stokes U profiles formed along rays lying in a fixed plane (Fig. 4 c) does not differ substantially from that of Stokes Q . In particular, the U -profile evolves in phase with Q . In contrast to Stokes Q , however, the sign of U corresponds to the sign of l_x , i.e. the U profiles coming from the right and left halves of the flux tube have opposite sign (see Appendix B for an explanation). The change of sign causes significant differences between the two Stokes parameters. Whereas spatially averaged Q profiles have a similar form to the spatially resolved profiles, this is not the case for Stokes U . Spatially averaged U profiles can be far more complex than their spatially resolved constituents.

In order to help understand the spatial average we display in Fig. 7a Stokes U profiles at phase 0.25 originating at $l_x \geq 0$. The solid line in Fig. 7a denotes the signal at $l_x = 0$. It is symmetric due to the vanishing line-of-sight velocity and positive since it is produced purely by magneto-optical effects. The profiles at $l_x \sim 50$ km (dashed line) and 100 km (dash-dotted line) have larger amplitude than at $l_x = 0$ whereas profiles at $l_x > 100$ km (dash-triple-dotted line) decrease in magnitude. The increase in a_σ from $l_x = 0$ to 100 km is due to $B_{rx} \sim l_x$, i.e. due to the increasing χ with l_x (cf. Sect. 2.3, note that χ never exceeds 45°). The decrease at larger $|l_x|$ reflects, as for Q and V , the decreasing intersection area of the flux tube with the plane containing the lines-of-sight (cf. Sect. 3.2.2).

The average of the U profiles formed over the whole flux tube is displayed in Fig. 7b (solid curve). For comparison the spatially averaged profile calculated without magneto-optical effects is also plotted (dashed curve). Noteworthy are the small amplitudes of these profiles (compared to the amplitudes of some of the profiles in Fig. 7a), as well as their complex and asymmetric shapes. In particular, the profile calculated without

magneto-optical effects is almost antisymmetric and appears more like a combination of two shifted Stokes V profiles. Both the reduced amplitude and complex shape are due to the addition of Stokes U profiles having opposite sign originating from the two halves of the flux tube. Their cancellation leads to the small amplitude. Also, profiles resulting from planes with opposite l_x are wavelength shifted in opposite directions and have different amplitudes. Therefore, they do not cancel each other exactly but build up complex profile shapes. When magneto-optical effects are neglected, Stokes U is proportional to $\sin 2\chi$ (Eq. B9, see Appendix B) and the spatially averaged U profile is nearly antisymmetric according to wavelength. Note that this signal is completely caused by the wave, since in the absence of a wave the U profile of a vertical flux tube is entirely generated by magneto-optical effects. If these were switched off U would disappear in an untwisted, static flux tube. The inclusion of the magneto-optical effects introduces terms proportional to $\cos 2\chi$, which produce a U signal having the same sign in both halves of the flux tube. These terms are responsible for the predominantly positive U profile in Fig. 7b (solid curve).

Due to the complex shape (which makes it difficult to define profile parameters that may be directly compared with those of Stokes V and Q) and the small amplitude of the spatially averaged U profiles we do not discuss them further, although Stokes U reveals the clearest signal of the torsional waves of all spatially averaged Stokes parameters. Hence we encourage low-noise observations of Stokes U near the limb. Note that in Fig. 7 we have concentrated on the phase 0.25 which, along with phase 0.75, produces the most asymmetric U profiles. Note also that spatially averaged Stokes U profiles fluctuate at the wave frequency in the sense that at all phases different profiles are generated. However, the U amplitude and width oscillate at twice the wave frequency, like the corresponding parameters of Stokes Q and V .

3.4. Temporally averaged parameters

In this section we discuss the signature of torsional waves of temporally (and spatially) averaged Stokes V and Q (Sect. 3.4.1) and U (Sect. 3.4.2) profiles. Note that averaging over time over a single flux tube corresponds approximately to spatially averaging over many flux tubes caught at random phases of the wave.

3.4.1. Stokes V and Q

Fig. 8 displays the dependence on \tilde{v} of the same line profile parameters as plotted in Fig. 6. The parameters are also shown for two heliocentric angles θ and two spectral lines. In the following each of these dependences is briefly discussed. Note that all in all the influence of the torsional wave agrees qualitatively with the findings for the kink wave (Fig. 8 of Paper I). The dependence of the signature on the wave frequency and amplitude, the heliocentric angle and spectral line does not differ qualitatively from that of a kink wave.

This includes the fact that the sign of the wavelength shift and asymmetry of Stokes V profiles is opposite to that of Stokes Q profiles. This effect is already seen in the spatially averaged but temporally resolved profiles, as discussed in Sect. 3.2.2. Since these parameters maintain their sign over most of the wave period (Fig. 6) the temporally averaged profiles inherit this property. Compared to the peak values in Fig. 6 the influence of the same wave on the time averaged parameters is small, partly due to the averaging and partly because at phases where the shift, asymmetry and broadening are large (phase 0.25 and 0.75 in Fig. 6) the V and Q amplitude is reduced.

Dependence on wave amplitude and frequency: As expected, the wave amplitude, \tilde{v} , plays a dominant role. The influence of the wave on all line parameters increases as \tilde{v} increases due to the increased velocity gradient. The role of the wave frequency ω is less important (and therefore not displayed). The larger the frequency the larger the ratio between the height–range over which the line is formed to the wavelength of the wave. This increases the line-of-sight gradients somewhat, producing a slightly larger asymmetry, but decreases parameter fluctuations over the wave period.

Dependence on limb-distance: The heliocentric angle θ determines firstly the line-of-sight velocity $v_{\text{los}} = v_y \sin \theta$ (Sect. 2.3) and secondly the sensitivity of the Stokes profiles with respect to changes in magnetic inclination γ (Sect. 3.2.2 and Paper I). Stokes V , whose parameters are displayed in the left panels of Fig. 8, shows the expected increase in shift, width and asymmetry from $\theta = 30^\circ$ to $\theta = 70^\circ$, because both the line-of-sight velocity and the sensitivity to γ -changes increases towards the limb. The V amplitude also decreases more strongly at $\theta = 70^\circ$, partly as a compensation for the increased line width: The decrease in σ -component area is much smaller. The behaviour of the Stokes Q line parameters reflects, on the one hand, the loss of sensitivity with respect to γ -changes toward the limb, and on the other hand the increased v_{los} . Hence, the line width, which is mainly sensitive to v_{los} , increases towards the limb (and the amplitude decreases). The line shift, however, decreases in magnitude towards the limb, while the asymmetry remains relatively unchanged.

Dependence on the spectral line. In Paper I we found that the line Fe I 5083 Å reacts more sensitively to the kink wave than Fe I 5250.2 Å. This is particularly true for δa and δA . We find that this is also the case for the torsional waves, as can be seen from Fig. 8. The main reason is again that Fe I 5083 Å is more saturated, which gives it a larger asymmetry (cf. Solanki 1989, Paper I).

3.4.2. Stokes U

Fig. 9 a shows the temporally and spatially averaged Fe I 5250 Å U profiles for $\tilde{v} = 1 \text{ km s}^{-1}$ (solid line), $\tilde{v} = 2 \text{ km s}^{-1}$ (dashed

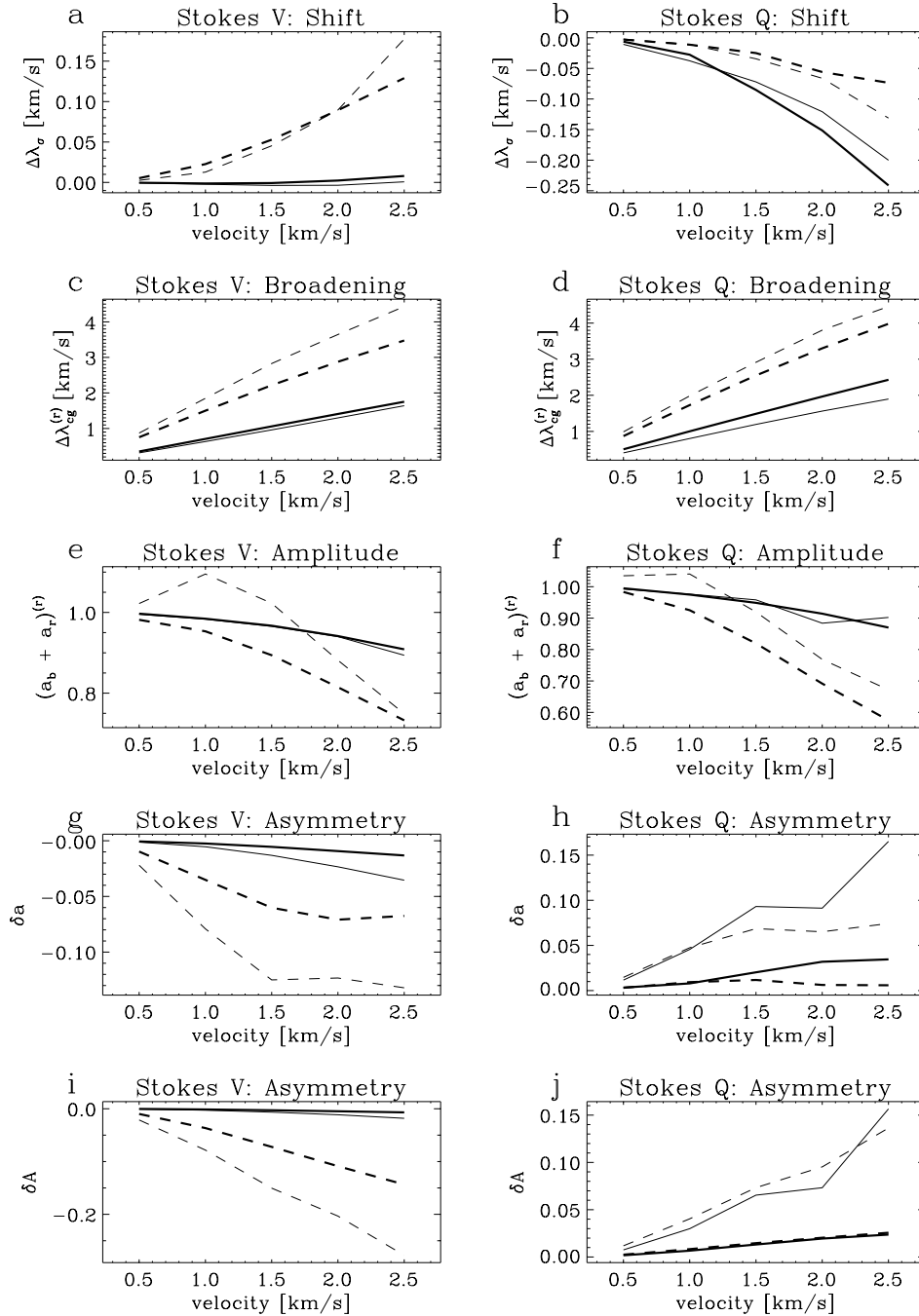


Fig. 8a–j. Temporally and spatially averaged line-profile parameters of Stokes V and Q vs. wave amplitude \tilde{v} . The parameters are displayed for two heliocentric angles ($\theta = 30^\circ$ solid, and $\theta = 70^\circ$ dashed) and two spectral lines (Fe I 5083 Å, thin lines and Fe I 5250.2 Å, thick lines).

line) and $\tilde{v} = 2.5 \text{ km s}^{-1}$ (dash-dotted line). As expected from Sect. 3.3 the U amplitude is far smaller than that of Q or V , but nevertheless slightly larger than the U generated without the wave. Note the increasing asymmetry with increasing \tilde{v} . These temporally averaged U profiles are more symmetric than the profiles at phase 0.25 and 0.75 shown in Fig. 7. Two effects are responsible for this: 1) at most other phases the U profiles are more symmetric 2) in the course of a wave period the asymmetry of U changes sign, so that averaging over these profiles leads to far smaller net asymmetry. The opposite sign of the asymmetry to that of Stokes Q reflects the different dependence of these profiles on χ in the presence of averaging.

Fig. 9b shows line profile at $\theta = 30^\circ$ (solid line), 60° (dashed line) and 80° (dash-dotted line) for Fe I 5250.2 Å. At large θ a residual effect of the wave is visible in the asymmetry of the profiles, whereas magneto-optical effects dominate the profiles at small θ .

4. Summary and conclusions

4.1. Summary of the results

In this study we investigate in detail the influence of torsional Alfvén waves in solar magnetic flux tubes on Stokes profiles.

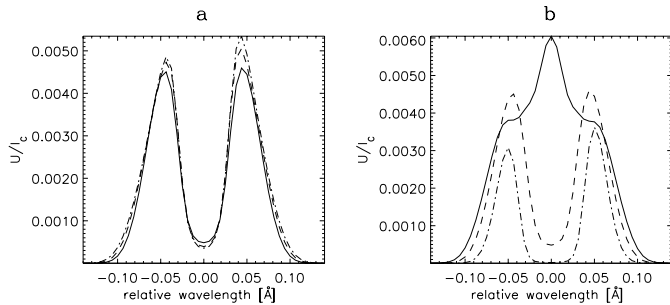


Fig. 9a and b. Temporally and spatially averaged line profiles of Stokes U for different \tilde{v} and θ . The profiles displayed in frame **a** correspond to wave amplitudes $\tilde{v} = 1 \text{ km s}^{-1}$ (solid line), $\tilde{v} = 2 \text{ km s}^{-1}$ (dashed line) and $\tilde{v} = 2.5 \text{ km s}^{-1}$ (dash-dotted line), those in frame **b** to $\theta = 30^\circ$ (solid), $\theta = 60^\circ$ (dashed) and $\theta = 80^\circ$ (dash-dotted).

We have used basically the same methods as for our earlier investigations of longitudinal (Solanki & Roberts 1992) and kink waves (Ploner & Solanki 1997 called Paper I), i.e. we simply overlaid linear torsional waves calculated for isothermal, thin flux tubes onto realistic model atmospheres of the flux tube and its surroundings. At each time step over a wave period we then calculated line profiles along sets of inclined rays passing through the flux tube. In contrast to the kink wave it is extremely important to also include rays that do not pass through the flux-tube axis when considering torsional waves.

The shift, width and asymmetry of the Stokes profiles fluctuate according to the line-of-sight velocity. Their amplitude changes following the direction of the magnetic field vector. For profiles formed along the rays lying in a single vertical plane offset by l_x from the flux-tube axis (see Fig. 1) the variations are similar to those produced by kink waves (Paper I). The magnitude of the profile variations, however, depends strongly on l_x since the line-of-sight velocity v_{los} is proportional to l_x in our model. The line shift, broadening and asymmetry parameters vanish for $l_x = 0$ (i.e. in a plane passing through the flux-tube axis) and increase rapidly with increasing $|l_x|$. The magnitude a_σ of the profiles has the opposite dependence on l_x since the flux tube fills increasingly smaller parts of the atmosphere there: the intersection of the flux tube with the plane containing the lines-of-sight decreases with $|l_x|$.

The *spatially averaged* (but temporally resolved) profiles of V and Q follow the wave with double the wave frequency because, due to the azimuthal symmetry of the wave perturbations, the left and right halves of the flux tube (as seen from an inclined observer) are exactly half a period out of phase. Half a wave period later the wave perturbations in the two halves are interchanged and lead to the same average line parameters (except for perturbations caused by magneto-optical effects).

Although profiles generated in outer (i.e. large $|l_x|$) planes are heavily distorted the spatially averaged profiles show only a moderate influence of the wave since they obtain their major contribution near the central plane. The wavelength shift and asymmetry of the spatially averaged Stokes V and Q have opposite signs. This has the same cause as that underlying the opposite signs of the same line parameters of the temporally

averaged V and Q profiles in the presence of a kink wave (Paper I).

The behaviour of Stokes U differs from the other Stokes profiles because in U the σ -components can be positive or negative according to the sign of l_x (and are therefore small near $l_x = 0$). The spatially averaged U -profiles are found to be weak in amplitude, rather complex in shape and asymmetric.

Unsurprisingly, *spatially* and *temporally averaged* profiles are even less affected by the wave (except for line broadening). We find that all effects of the wave seen in the line-profile parameters are enhanced by the wave's amplitude \tilde{v} , whereas the wave frequency plays only a minor role. The perturbations in Stokes V and Q due to the wave have opposite centre-to-limb variations. The asymmetries and line shift are largest at the limb for Stokes V , but closer to disc centre for Stokes Q .

4.2. Comparison between kink and torsional wave

Let us first consider temporally resolved but spatially averaged Stokes V and Q profiles. One major difference between the two wave modes is that the oscillations in Stokes V and Q reflect the frequency of the kink wave but double the wave frequency of torsional waves. In addition, line shift and asymmetry parameters influenced by torsional waves have a unique sign at all phases (positive for Stokes Q and negative for V). In contrast, the parameters affected by kink waves oscillate around zero. Also, for similar wave velocities, torsional waves shift the line profiles by less than half as much as kink waves do. The oscillation amplitudes and absolute values of the asymmetries are also significantly reduced (by up to a factor of 6). The temporal average does not alter the above points significantly. The dependence of the V and Q parameters on the wave amplitude and frequency and on the position on solar disc is basically the same for both waves.

That torsional waves affect polarized line profiles less strongly than kink waves has the following three reasons, which all root in the different nature of the waves.

1. The phase velocity of torsional waves is $v_A = B/\sqrt{4\pi\rho}$ and is larger than that of the kink wave $v_k \sim B/\sqrt{4\pi(\rho + \rho_{ex})}$ because the latter is influenced by the density ρ_{ex} of the external atmosphere which, for typical flux-tube parameters, is significantly larger than the density inside the tube ρ . The wave-induced field inclination is consequently larger for kink than for torsional waves if an equal wave-velocity amplitude is assumed. (Compare with Eq. 6.)
2. The velocity induced by a kink wave is oriented in a single direction and has constant magnitude within a flux-tube cross-section. In contrast, the velocity induced by a torsional wave is azimuthal and its amplitude is proportional to the distance to the centre (to first order). Assume that the velocity amplitude v of the kink wave agrees with the velocity amplitude of the torsional wave at the flux-tube boundary R_0 , $v = v_{\varphi 1} R_0$, where $v_{\varphi 1}$ is the angular velocity. In that case the average velocity within a cross section of the flux tube is $2/3$ of that of a kink wave. Note that the maximum

apparent velocity (assumed for $\theta = 90^\circ$) is $v_y = v_{\phi 1} l_x$ (Eq. 10) and that consequently only $4/(3\pi) \sim 0.42$ of a constant and isotropic velocity v can actually be seen by the radiative transfer equation. For the velocity field assumed above the energy flux (the product of kinetic energy and phase velocity) is roughly the same for kink and torsional waves (this assumes that the external density is four times the internal density or that the phase velocity of kink waves is half of the Alfvén speed).

3. The degree of polarization strongly depends on the path the light takes through the flux tube. The amount of magnetic material along a ray is largest if it intersects the flux-tube axis, but rapidly decreases as the shortest distance between the ray and the axis increases. Consequently, most of the polarized light stems from close to the flux-tube axis. The torsional velocity, however, is small there, so that the kink wave only has a small influence on the Stokes parameters formed there.

The largest consequence of the difference for the observational detection of these waves is that for a given wave energy flux it is far easier to detect a kink wave than a torsional wave by its signature in the Stokes parameters. Hence, the constraints set by observations on the wave flux (which will be the subject of another paper) is expected to be less tight for torsional waves than for kink or longitudinal waves.

Acknowledgements. This work has been supported by grant No. 20-43048.95 of the Swiss National Science Foundation. We thank M. Schüssler for very helpful discussions on torsional waves.

Appendix A: line profile parameters

The *line shift* is defined as $\Delta\lambda_\sigma = \frac{1}{2}(\lambda_r + \lambda_b)$, where $\lambda_{r,b}$ is the wavelength of the red, respectively blue σ -component peak. The *line broadening* is the difference between the centre-of-gravity wavelengths of the blue and red σ -components:

$$\Delta\lambda_{cg} = \frac{1}{2} \left(\frac{\int_{\text{red}} \Delta\lambda |s(\lambda)| d\lambda}{\int_{\text{red}} |s(\lambda)| d\lambda} - \frac{\int_{\text{blue}} \Delta\lambda |s(\lambda)| d\lambda}{\int_{\text{blue}} |s(\lambda)| d\lambda} \right).$$

The function $s(\lambda)$ stands for V , Q , or U and $\Delta\lambda$ for the unsigned wavelength relative to line-centre. We isolate the effects of the wave by removing the width of the reference profile (i.e., the corresponding Stokes profile calculated in the absence of the wave) according to $\sqrt{\Delta\lambda_{cg}^2 - \Delta\lambda_{cg,ref}^2}$. The unsigned σ -component amplitudes are $a_\sigma = a_b + a_r$ (where a_b and a_r indicate the blue and red σ -components, respectively). In order to stress the variations the total amplitude is normalized to the amplitude $a_{\sigma,ref}$ of the reference profile: $a_\sigma/a_{\sigma,ref}$. The *relative amplitude* and *area asymmetry* are defined as

$$\delta a = \frac{a_b - a_r}{a_b + a_r}, \quad \delta A = \frac{A_b - A_r}{A_b + A_r},$$

respectively. Here, A_b and A_r are the unsigned areas of the blue and red σ -components, respectively.

Appendix B: analytical considerations based on a Milne-Eddington atmosphere

In this Appendix we use analytical solutions of the polarized radiative transfer equations, including the magneto-optical effects, describing a Zeeman-split line in a Milne-Eddington atmosphere to explicate the dependence of the V , Q and U profiles on γ and χ . The solutions (due originally to Rachkovsky, 1967) are taken from, e.g., Arena & Landi degl'Innocenti (1982) and read

$$Q/I_c \sim \eta_Q (\eta_I + 1)^2 + \varrho_Q s + (\varrho_V \eta_V - \varrho_V \eta_U) (\eta_I + 1), \quad (\text{B1})$$

$$U/I_c \sim \eta_U (\eta_I + 1)^2 + \varrho_U s + (\varrho_V \eta_Q - \varrho_Q \eta_V) (\eta_I + 1), \quad (\text{B2})$$

$$V/I_c \sim \eta_V (\eta_I + 1)^2 + \varrho_V s, \quad (\text{B3})$$

$$s = \eta_Q \varrho_Q + \eta_U \varrho_U + \eta_V \varrho_V.$$

Here $s = \eta_Q \varrho_Q + \eta_U \varrho_U + \eta_V \varrho_V$, while the η_p (with $p = I, V, Q$, or U) are defined as

$$\eta_I = \left(\frac{1}{2} \eta_0 \sin^2 \gamma - \frac{1}{4} (\eta_{+1} - \eta_{-1}) (1 + \cos^2 \gamma) \right), \quad (\text{B4})$$

$$\eta_Q = \left(\frac{1}{2} \eta_0 - \frac{1}{4} (\eta_{+1} - \eta_{-1}) \right) \sin^2 \gamma \cos 2\chi, \quad (\text{B5})$$

$$\eta_U = \left(\frac{1}{2} \eta_0 - \frac{1}{4} (\eta_{+1} - \eta_{-1}) \right) \sin^2 \gamma \sin 2\chi, \quad (\text{B6})$$

$$\eta_V = \left(\frac{1}{2} (\eta_{+1} - \eta_{-1}) \right) \cos \gamma. \quad (\text{B7})$$

The definitions of the ϱ_p are obtained if in Eqs. (B5)–(B7) η is replaced by ϱ . Each η_i (with $i = 0, \pm 1$) is basically a Voigt function and ϱ_i a Faraday function (e.g. Landi degl'Innocenti 1976), but their precise functional form does not play a role for the present purpose. If we introduce $\eta_a = \frac{1}{2} \eta_0 - \frac{1}{4} (\eta_{+1} - \eta_{-1})$ and $\eta_b = \frac{1}{2} (\eta_{+1} - \eta_{-1})$, as well as the similarly defined quantities ϱ_a and ϱ_b , then Eqs. (B1)–(B3) read

$$Q/I_c \sim \sin^2(\gamma) \cos(2\chi) ((\eta_I + 1)^2 \eta_a + s \varrho_a) + \sin^2(\gamma) \cos(\gamma) \sin(2\chi) (\varrho_a \eta_b - \varrho_b \eta_a) (\eta_I + 1), \quad (\text{B8})$$

$$U/I_c \sim \sin^2(\gamma) \sin(2\chi) ((\eta_I + 1)^2 \eta_a + s \varrho_a) + \sin^2(\gamma) \cos(\gamma) \cos(2\chi) (\varrho_a \eta_b - \varrho_b \eta_a) (\eta_I + 1), \quad (\text{B9})$$

$$V/I_c \sim \cos(\gamma) ((\eta_I + 1)^2 \eta_b + s \varrho_b), \quad (\text{B10})$$

$$s = \eta_a \varrho_a \sin^4 \gamma + \eta_b \varrho_b \cos^2 \gamma.$$

Note that since η_i and ϱ_i are independent of γ and χ , so are η_a , η_b , ϱ_a and ϱ_b . η_I and s in (B8)–(B10) still depend on γ , but all χ dependences are explicitly written in the $\sin 2\chi$ and $\cos 2\chi$ terms. In Eqs. (B8) to (B10) the terms proportional to $(\eta_I + 1)^2$ generally give the bulk of the signal and the terms proportional to $(\eta_I + 1)$ are due exclusively to the magneto-optical effects. Except very close to the limb γ does not cause a change in sign of any terms. The azimuth χ , in contrast, has opposite signs in the left and right halves of the flux tube (as seen from the vantage point of the observer). Eq. (B8) then predicts that the Stokes Q

amplitude has the same sign for both $+l_x$ and $-l_x$: Q/I_C is dominated by $\cos(2\chi)$ while the magneto-optical effects introduce a weaker dependence on $\sin(2\chi)$. Stokes U , however, has the reversed dependence on χ according to Eq. (B8) the bulk of the signal is proportional to $\sin(2\chi)$ and only the magneto-optical effects give a term proportional to $\cos(2\chi)$. Finally, Stokes V remains independent of χ in this approximation.

References

- Anton V., 1989, Dissertation, Göttingen (in german)
- Arena P., Landi degl'Innocenti E., 1982, A&AS 48, 81
- Bünte M., Solanki S.K., Steiner O., 1993, A&A 268, 736
- Fawzy D.E., Ulmschneider P., Cuntz M., 1998, A&A 336, 1029
- Ferriz Mas A., Schüssler M., Anton V., 1989, A&A 210, 425
- Frutiger C., Solanki S.K., 1998, A&A 336, L65
- Gandorfer A.M., Povel H.P., 1997, A&A 328, 381
- Grossmann-Doerth U., Schüssler M., Solanki S.K., 1989, A&A 221, 338
- Herbold G., Ulmschneider P., Spruit H.C., Rosner R., 1985, A&A 145, 157
- Huang P., Musielak Z.E., Ulmschneider P., 1995, A&A 279, 579
- Landi degl'Innocenti E., 1976, A&AS 25, 379
- Maltby P., Avrett E.H., Carlsson M., et al., 1986, ApJ 306, 284
- Martínez Pillet V., Lites B.W., Skumanich A., 1997, ApJ 474, 810
- Nakariakov V.M., Roberts B., Murawski K., 1997, Sol. Phys. 175, 93
- Narain U., Ulmschneider U., 1990, Space Sci. Rev. 54, 377
- Narain U., Ulmschneider U., 1996, Space Sci. Rev. 75, 453
- Ploner S.R.O., Solanki S.K., 1997, A&A 325, 1199
- Poedts S., Beliën A.J.C., Goedbloed J.P., 1994, Sol. Phys. 151, 271
- Povel H.-P., 1995, Optical Engineering 34, 1870
- Rachkovsky D.N., 1967, Izv. Krymsk. Astrofiz. Obs. 37, 56
- Rammacher W., 1991, In: Ulmschneider P., Priest E.R., Rosner R. (eds.) Mechanisms of Chromospheric and Coronal Heating. Springer Verlag, Heidelberg, p. 414
- Rammacher W., Ulmschneider P., 1989, In: Rutten R., Severino G. (eds.) Solar and Stellar Granulation. Reidel, Dordrecht, p. 589
- Roberts B., Ulmschneider P., 1996, In: Simnett G.M., Alisandrakis C.E., Vlahos L. (eds.) Solar and Heliospheric Plasma Physics. Springer, Heidelberg, p. 75
- Rüedi I., Solanki S.K., Livingston W., Stenflo J.O., 1992, A&A 263, 323
- Solanki S. K., 1989, A&A 224, 225
- Solanki S.K., 1996, In: Simnett G.M., Alisandrakis C.E., Vlahos L. (eds.) Solar and Heliospheric Plasma Physics. Springer, Heidelberg, p. 49
- Solanki S.K., Brigljević V., 1992, A&A 262, L29
- Solanki S.K., Pahlke K.D., 1988, A&A 201, 143
- Solanki S.K., Roberts B., 1992, MNRAS 256, 13
- Spruit H.C., 1982, Sol. Phys. 75, 3
- Steiner O., Grossmann-Doerth U., Knölker M., Schüssler M., 1995, Rev. Modern Astron. 8, 81
- Steiner O., Grossmann-Doerth U., Schüssler M., Knölker M., 1996, Sol. Phys. 164, 223
- Ulmschneider P., Musielak Z.E., 1998, A&A 338, 311
- Ulrich R.K., 1996, ApJ 465, 436
- Venkatakrishnan P., 1993, Sol. Phys. 148, 233
- Webb A.R., Roberts B., 1980, Sol. Phys. 68, 71
- Zähringer K., Ulmschneider P., 1987, In: Schröter E.H., Vazquez M., Wyller A.A. (eds.) The Role of Fine-Scale Magnetic Fields on the Structure of the Solar Atmosphere. Cambridge Univ. Press, Cambridge, England, p. 49
- Zhugzhda Y.D., 1996, Physics of Plasmas 3, 10
- Ziegler U., Ulmschneider P., 1997a, A&A 324, 417
- Ziegler U., Ulmschneider P., 1997b, A&A 327, 854